Ganguli, P., Merz, B. (2019): Trends in Compound Flooding in Northwestern Europe During 1901–2014. - *Geophysical Research Letters*, *46*, 19, pp. 10810—10820.

DOI: http://doi.org/10.1029/2019GL084220

Geophysical Research Letters

RESEARCH LETTER
10.1029/2019GL084220

Trends in Compound Flooding in Northwestern Europe During 1901–2014

Poulomi Ganguli[1,2] **and Bruno Merz**[2,3]

[1]Agricultural and Food Engineering Department, Indian Institute of Technology Kharagpur, Kharagpur, India, [2]German Research Centre for Geosciences (GFZ), Potsdam, Germany, [3]Institute for Environmental Sciences and Geography, University of Potsdam, Potsdam, Germany

Key Points:
- We analyze space-time trends in compound flooding in northwestern Europe during 1901–2014 using compound hazard ratio index
- We show a spatially coherent pattern in compound flood magnitude and frequency in middle and high latitudes in northwestern Europe
- Our analysis reveals upward trends in compound flood frequency for larger return levels at stream gauges across middle latitudes

Supporting Information:
- Supporting Information S1

Correspondence to:
P. Ganguli,
pganguli@agfe.iitkgp.ac.in;
poulomizca@gmail.com

Citation:
Ganguli, P., & Merz, B. (2019). Trends in compound flooding in northwestern Europe during 1901–2014. *Geophysical Research Letters*, *46*, 10,810–10,820. https://doi.org/10.1029/2019GL084220

Received 21 JUN 2019
Accepted 9 SEP 2019
Accepted article online 12 SEP 2019
Published online 11 OCT 2019

Abstract We analyze trends in compound flooding resulting from high coastal water levels (HCWLs) and peak river discharge over northwestern Europe during 1901–2014. Compound peak discharge associated with 37 stream gauges with at least 70 years of record availability near the North and Baltic Sea coasts is used. Compound flooding is assessed using a newly developed index, compound hazard ratio, that compares the severity of river flooding associated with HCWL with the at-site, T-year (a flood with $1/T$ chance of being exceeded in any given year) fluvial peak discharge. Our findings suggest a spatially coherent pattern in the dependence between HCWL and river peaks and in compound flood magnitudes and frequency. For higher return levels, we find upward trends in compound hazard ratio frequency at midlatitudes (gauges from 47°N to 60°N) and downward trends along the high latitude (>60°N) regions of northwestern Europe.

Plain Language Summary Compound floods in delta areas, that is, the co-occurrence of high coastal water levels (HCWLs) and high river discharge, are a particular challenge for disaster management. Such events are caused by two distinct mechanisms: (1) HCWLs may affect river flows and water levels by backwater effects or by reversing the seaward flow of rivers, particularly in regions with elevation less than 10 m in northwestern Europe. (2) The correlation between HCWL and river flow peaks may also stem from a common meteorological driver. Severe storm periods may be associated with high winds leading to storm surges, and at the same time with high precipitation followed by inland flooding. Understanding the historical trends in compound flooding, owing to changes in relative sea levels, in river flooding and in the dependence between these two drivers, is essential for projecting future changes and disaster management. The risk assessment frameworks are often limited to assessing flood risk from a single driver only. We present a new approach to assess compound flood severity resulting from extreme coastal water level and peak river discharge. We find upward trends in compound flooding for midlatitude regions and downward trends for high latitudes in northwestern Europe.

1. Introduction

There is a considerable body of recent literature on compound flooding, that is, the simultaneous or d-day lagged occurrence of extreme sea levels and peak river discharges (or extreme precipitation as a proxy for flooding), in Europe (Bevacqua et al., 2017; Bevacqua et al., 2018; Paprotny et al., 2018; Petroliagkis et al., 2016) and globally (Moftakhari et al., 2017; Wahl et al., 2015; Ward et al., 2018; Zheng et al., 2013; Zscheischler et al., 2018). Compound flooding may lead to significant impacts and much more disastrous consequences than each of these extremes individually (Leonard et al., 2014). Previous researchers have identified a moderate to strong correlation between high coastal water levels (HCWLs) or storm surges and floods (either pluvial or fluvial) globally (Ward et al., 2018), and regionally across Europe (Kew et al., 2013; Paprotny et al., 2018; Petroliagkis et al., 2016; Reeve et al., 2008; Svensson & Jones, 2001; Svensson & Jones, 2004), the United States (Moftakhari et al., 2017; Sadegh et al., 2018), Australia (Wu et al., 2018; Zheng et al., 2013, 2014), and China (Lian et al., 2013; Tu et al., 2018). In addition, they have focused on the joint probability of compound floods (Couasnon et al., 2018; Kew et al., 2013; Moftakhari et al., 2019; Moftakhari et al., 2017; Sadegh et al., 2018; Ward et al., 2018) considering individual drivers and the conditional probability (Bevacqua et al., 2017) of occurrence of river floods given moderate to extreme coastal water levels or surges. These metrics are valuable for risk management and infrastructure design in delta areas (Wu et al., 2018).

Regions at the mouth of big rivers, home to around 33 million people in northwestern Europe (Neumann et al., 2015), are threatened by relative sea level (RSL) rise, a consequence of climate change-induced increase and deltaic subsidence through groundwater abstraction or soil compaction by urban growth (Best, 2018). Compound floods at the vicinity of the coasts may results from two distinct mechanisms. First, HCWL may affect river flows and water levels by backwater effects or by reversing the seaward flow of rivers. The tidal signal may propagate as much as over 500 km inland, increasing flood risk far from the coast (Hoitink & Jay, 2016). Rivers in the regions with elevation less than 10 m in northwestern Europe (Figure 1 in Hoitink & Jay, 2016) are likely to be influenced by this mechanism. Second, the dependence between HCWL and river flow peaks may also stem from a common meteorological cause. Severe storm periods may be associated with high winds leading to storm surges, and at the same time with high precipitation followed by inland flooding (Kew et al., 2013). The coincidence of these hydroclimatic drivers in space and time exacerbate flood impacts (Field et al., 2012; Leonard et al., 2014).

Temporal changes in compound flooding may follow from changes in HCWL, river floods, and changes in the dependence between these two drivers. RSL trends, derived from tide gauge (TG) observations along the European coasts, show a general increase in mean local sea levels, and hence, extreme coastal water levels, but significant regional variations exist. Along the North Sea coast, RSL has increased with significantly higher rates than the global mean in the recent decades (Wahl et al., 2013), whereas the opposite is observed for the northern Baltic Sea coast and the northern Atlantic coast, in which RSLs have been showing a decreasing trend owing to considerable land rise as a consequence of postglacial rebound (EEA, 2017; Richter et al., 2012; Wahl et al., 2013). Trends in peak-over-threshold river floods across Europe show spatially coherent patterns, with a tendency toward significant upward trends in flood magnitude and frequency in the Atlantic region covering the entire United Kingdom, Netherlands, Denmark, and the coastal regions in Germany and France. On the other hand, an increasing number of flood events with decreasing flood magnitude are observed for the Boreal (covering most of Scandinavia) climatic region (Mangini et al., 2018).

Despite quantifying the correlation between HCWL (or surges) and river discharge (or extreme precipitation) in the vicinity of the coast, none of the studies so far has assessed the expected T-year peak river discharge given HCWL during severe storm episodes, especially in winter (November–February), when strong north or northwesterly winds are present over the North Sea. The opposite, that is, the influence of river discharge on coastal ocean circulation, and therefore RSL variations, has been shown for the U.S. Atlantic coast (Meade & Emery, 1971; Piecuch et al., 2018). On the other hand, HCWL plays a direct role in river flow propagation since the unsteady river flow follows a subcritical flow regime, which is impacted by both upstream and downstream boundary conditions. The coastal ocean forms the downstream boundary of a river that causes both river stage and flow discharge to be influenced by RSL variations, tides, and storm surges (Hoitink & Jay, 2016). To the best of our knowledge, while earlier assessments (Burn & Whitfield, 2018; Gudmundsson et al., 2018; Mangini et al., 2018; Mediero et al., 2015; Stocker, 2014) were tailored to univariate flood trends, this is the first attempt to analyze trends in the co-occurrence of fluvial floods and extreme coastal water levels and their regional pattern. Second, we develop a dimensionless index, compound hazard ratio (CHR), that links peak river discharge to HCWLs.

We use multivariate extreme value theory in a Bayesian framework (Cheng & AghaKouchak, 2014; Cheng et al., 2014) to infer the large-scale (northwestern European coast) space-time structure of compound flood trends during 1901–2014. Inferences are based on high-frequency RSL observations from TGs (Woodworth et al., 2016) and the longest and high-quality daily stream flow (Grabs, 1997) records along northwestern Europe. Along the North Atlantic coast, the majority of high tide flooding occurs in response to both tidal forcing during spring tides and a meteorologically driven component, such as storm surges (Haigh et al., 2016; Sweet et al., 2018). A compound flood event is determined as a joint occurrence of hourly annual maxima coastal water level (as an indicator of HCWL; Bevacqua et al., 2018; Moftakhari et al., 2017; Sadegh et al., 2018; Sweet et al., 2018) and the lagged daily fluvial peak discharge within a 500-km radius of TGs (Bartsch-Winkler & Lynch, 1988; Hoitink & Jay, 2016) in a time range of ± 7 days from the day of occurrence of the HCWL event. The lag time of the discharge is determined using the average response time of the catchment to a precipitation event (see section 2). A lag of a few days has been considered only in a limited number of studies (Klerk et al., 2015; Kew et al., 2013; Petroliagkis et al., 2016; Zheng et al., 2017) but has been neglected in several other assessments (Bevacqua et al., 2018; Moftakhari et al., 2017; Reeve et al., 2008; Sadegh et al., 2018; Svensson & Jones, 2004; Tu et al., 2018; Wahl et al., 2015).

2. Methodology

We quantify the temporal variability in compound flooding at 35-year (climate timescale; WMO, 2017) moving windows, shifted by 1 year at each time step (Brunetti et al., 2001; Ghosh et al., 2012; Kharin et al., 2007; Ntegeka & Willems, 2008). The choice of the window length is the trade-off between short enough intervals to ensure stationarity of variables (with no significant trends) and a sufficient sample size to quantify the dependence structure. For each of the moving windows, we estimate the nonparametric dependence measures, Kendall's τ, and empirical upper tail dependence metric (Capéraá-Fougéres-Genest [CFG] estimator, λ_{CFG}; see section S1.1 in the supporting information) between the flood drivers within $\pm$7 days of the HCWL event. Although HCWL and river peaks may be caused or influenced by the same event, they may not occur on the same day. Hence, a time window is required to consider this effect (Berghuijs et al., 2019; Czajkowski et al., 2017; Merz et al., 2018; Rowe & Villarini, 2013). Flood peaks that occur within a window of $\pm$7 days typically belong to the same large-scale event (Merz et al., 2018). The upper tail dependence metrics together with extreme value theory methods (Coles, 2001) are tools to infer the tail behavior of a sample. We then use copulas (Nelsen, 2013) to model trends in fluvial flood severity conditioned on HCWL. Our modeling framework is shown in Figure S1.

2.1. Coastal Water Level Data

We obtain RSL records from the longest hourly with at least 70 years of available sea level (in meter) observations (except Brest in France) in four of the TGs on the northwestern European (approximately from 46° to 66°N and from −12.5°W to 19°E) coast line (Table S1): Cuxhaven (Germany), Newlyn (United Kingdom), Brest (France) along the North Sea coast, and Stockholm (Sweden) along the Baltic Sea coast. Each of the TG contains more than 100 years of high-quality RSL records since the 1900s. The hourly RSLs of the TGs take into account tidal and nontidal processes (such as skew surge and nontidal residuals), whereas wave effects do not affect water level observations (Melet et al., 2018; Sweet et al., 2018), because TGs are typically located in sheltered locations that limit direct impact of winds relative to open coastlines. The TG at Newlyn contains RSL records at higher sampling frequencies (15 min) from 1993 onward. For consistencies, observations at higher sampling frequencies were averaged to hourly resolution by calculating the median of the quarterly values within each hour.

2.2. River Discharge Data

Daily continuous river discharge data (Global Runoff Data Centre [GRDC]; Grabs, 1997) from 39 stream gauges (SGs) with at least 70 years of record availability (since 1800s) near the North and Baltic Sea coasts are used to investigate long-term trends in compound flooding. For France, most of the SGs contain short discharge records starting from 1960s except Loire (at Montjean, catchment area = 109,930 km^2 and located at a geodesic distance of ~295 km from Brest) for which the daily continuous discharge data are available from 1843 onwards and were retrieved from the archived database Banque-Hydro website (http://www.hydro.eaufrance.fr/). The streamflow records from GRDC are originally provided by the national water agencies and have undergone quality control by GRDC. In general, discharge is estimated using rating curves assuming a relationship between water level and discharge. Both steady and unsteady rating curve models are prone to uncertainties owing to backwater effects from river-tide interactions, rapidly changing flow regime and other factors, such as seasonal variations in the vegetation state (Di Baldassarre & Montanari, 2009; Hidayat et al., 2011).

We select SGs within a radius of d = 500 km from the TGs. The choice of the d was based on previous literature (Hoitink & Jay, 2016) that suggests that the landward limit of tidally reversing currents is about 200 km inland and the tidal motion may propagate typically as far as 630 km (e.g., in River Yangtze) to over 1,000 km (e.g., in River Amazon) inland during low-flow periods. Finally, we compute the CHR for 37 gauges, since two of the gauges stem from the same river basin, and we select the one with the longer record.

2.3. Compound Event Identification

To identify compound flood events, first we calculate the annual maxima values from RSL records. Then for each individual SG, we shift the discharge time series by a basin lag time as dictated by the catchment-specific watershed response time. While HCWLs due to storm surges are frequently associated with synoptic low-pressure systems and onshore winds, a moisture-laden air mass in the catchment leads to extreme precipitation causing riverine flooding. Analyzing 32 European river mouths, Petroliagkis et al. (2016)

found that a lag time of a few days was required to establish a moderate to a strong correlation between surge and river discharge. We adopt a lag time considering the time elapsed to propagate rain-induced runoff at the downstream as a flood hydrograph (Leopold, 1991). We estimate lag time based on the catchment area (in km^2), A_D (Berne et al., 2004; Holtan & Overton, 1963):

$$d = 2.51A_d^{0.4}[\text{hrs}] = 0.11A_d^{0.4}[\text{days}]. \quad (1)$$

Finally, for each TG-SG pair, we search for the highest peak discharge of the shifted stream flow time series within an interval of $\pm$7 days of occurrence of the HCWL event. Hence, compound floods could results from (Pescaroli & Alexander, 2018) (1) extremes combined with background conditions amplifying the overall impact (Mechanism I); (2) extremes that occur simultaneously or successively (Mechanism II); and (3) extremes that result from a combinations of average conditions of either of the stressors, because in HCWL-peak discharge pairs, the later does not necessarily need to be an annual maxima event.

2.4. Dependence Between HCWL and Peak Discharge Time Series

We compute the complete dependence between TG-SG pairs using nonparametric Kendall's τ statistics and the extremal dependence using the empirical upper tail dependence coefficient determined from CFG estimator (λ_{CFG}) at a moving time (35-year) window series. We preferred the rank-based Kendall's τ over Spearman's ρ since the former offers better estimates of population parameter with smaller asymptotic variance; it is, hence, less susceptible to outliers (Chok, 2010). The statistical significance of dependence metrics is evaluated by drawing $N = 10{,}000$ random bootstrap samples from HCWL-peak discharge pair and calculating the p value of the test (i.e., probability of observing a stronger correlation by chance). We report statistical significance at 5% significance level.

2.5. Modeling Marginal Distribution of Compound Flood Variables

We fit the marginal distribution of compound flood drivers (i.e., HCWL and peak discharge) using Generalized Extreme Value (GEV) distribution (Bender et al., 2014; Tawn, 1992) to a moving time (35-year) window series. The GEV distribution is a combination of three different distributions, namely, Fréchet ($\zeta > 0$), Weibull ($\zeta < 0$), and the Gumbel ($\zeta \to 0$), depending on the sign of the shape (ζ) parameter. For estimation of GEV parameters, a Bayesian inference is performed combined with differential evaluation Markov Chain Monte Carlo simulation (Cheng & AghaKouchak, 2014; Martins & Stedinger, 2000; section S1.2). The validity of the fitted distribution is assessed by Kolmogorov-Smirnov and Cramer-von-Mises goodness-of-fit statistics at 5% significance level. Figures S2–S5 show marginal distribution fits of each of these compound flood drivers for a few selected SGs.

2.6. Time Series of CHR

The dimensionless multivariate index, CHR is defined as the ratio of the conditional T-year river peak discharge assuming HCWL as the covariate and the unconditional T-year seasonal maxima (November-March) peak discharge. *CHR* is expressed as

$$CHR = \frac{Q_T^{'}}{Q_T} = \frac{C^{-1}_{Q|HCWL=hcwl}\left[1-\frac{1}{T_{Q|HCWL}(q|hcwl)}\right]}{F_Q^{-1}\left[1-\frac{1}{T_Q(q)}\right]}, \quad (2)$$

where $T_{Q|HCWL}(q|hcwl) = \frac{1}{1-C_{Q|HCWL=hcwl}}$, where $Q_T^{'}$ denotes the conditional T-year peak discharge (Ganguli & Ganguly, 2016), $T_{Q\mid HCWL}$ indicates the conditional return periods considering HCWL as the covariate over 35-year moving window. Q_T indicates the unconditional at-site T-year peak discharge, T_Q. $C_{Q\mid HCWL=hcwl}$ indicates copula-based conditional distribution of peak discharge given $HCWL = hcwl$. $C^{-1}_{Q|HCWL=hcwl}$ and F_Q^{-1} denote inverse quantile transformation of copula-based and marginal (i.e., GEV in this case) distributions. First, we derive the copula-based conditional distribution of peak discharge for the given HCWL value at successive moving windows for each individual SG location. The index is motivated by the flood ratio approach (Czajkowski et al., 2017); Rowe & Villarini, 2013; Smith et al., 2011; Villarini & Smith, 2010) for the assessment of flooding associated with tropical cyclone-induced predecessor rain events. CHR offers the following improvements: (1) The use of copula allows considering nonlinear dependencies between drivers of compound floods. (2) Since for low-lying areas increasing HCWL due to RSL rise is a dominant factor, the conditional nature of CHR enables to model the influence of HCWL (Brunner et al., 2016) in

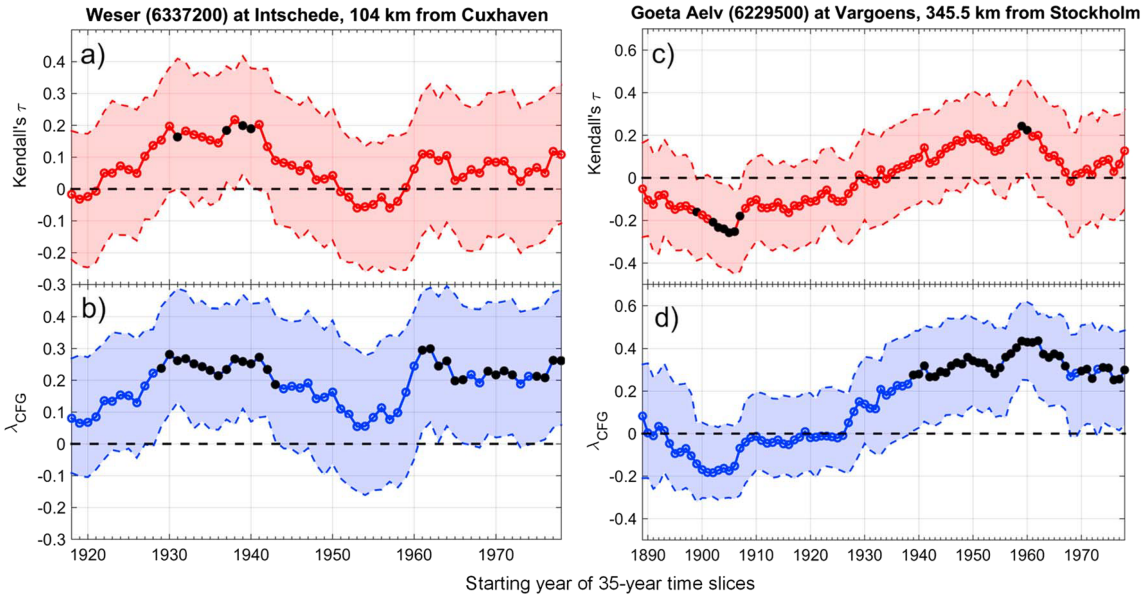

Figure 1. Temporal evolution of strength of dependence at the River Weser (a and b), Germany, along the North Sea and the River Göta Älv (c and d), Sweden, along the Baltic Sea coast. The top row shows complete dependence as measured by Kendall's τ, while the bottom row shows the nature of dependence at the upper tail of the bivariate extreme. The filled circles (in black) indicate statistically significant dependence at 5% significance level (p value < 0.05), obtained through 10,000 bootstrap simulations. The shaded bounds indicate the 95% confidence intervals simulated using the bootstrap resampling technique.

designing river flood defense. We derive CHR time series at individual SGs (equation (2)) over 35-year sliding windows. CHR = 1 shows a perfect agreement between conditional T-year peak discharge and univariate T-year river flood. CHR values larger (smaller) than 1 indicate that compound flood hazard is larger (smaller) than that of the seasonal at-site peak discharge, indicative of major (minor) flooding.

The CHR time series is calculated for each 35-year moving windows, assuming the midyear HCWL value as the conditioning variable to determine the expected T-year peak discharge for the given time slice. Since in northwestern Europe, the storm season (November–March) is often characterized by on average higher wind speeds, more pronounced storm activity, and high fluvial discharge (Feser et al., 2015; Kwadijk et al., 2016), we consider the seasonal peak discharge as the reference point to compare the severity of the compound flood. CHR is derived from the copula-based (Nelsen, 2013) conditional T-year return period (i.e., the specific event is expected to appear on average once in T year). Details of copula fitting and the selection of the particular copula family are discussed in the section S1.3. The graphical diagnostic plots of copula fit for illustrative sites, the River Wye (Gauge ID 6608501), United Kingdom, and the River Weser (Gauge ID 6337400), Germany, are presented (in Figures S6 and S7) as an evidence in favor of the selected bivariate distribution.

We compute CHR for $T = 50$- and 100-year return periods. The 50- and 100-year events can be considered as moderate-to-severe flood discharges that are often used for designing flood protection. We use nonparametric LOcally wEighted Scatter plot Smoothing (LOESS) regression smoothing to visualize space-time trends in compound flooding.

3. Results

3.1. Spatial Variability in Strength of Dependence Across Latitude

Figure 1 shows the temporal evolution of dependence along with 95% confidence intervals (obtained using 10,000 bootstrap simulations) at two representative SGs with longest available records at the North Sea and Baltic Sea coasts. Both dependence measures, Kendall's τ and λ_{CFG}, evolve synchronously. The moving window time series of UTDC shows statistically significant dependence from the 1930s to the mid-1950s and after 1960s for the River Weser-Cuxhaven TG pair. For the River Göta älv-Stockholm TG pair, significant dependence is observed after the 1940s.

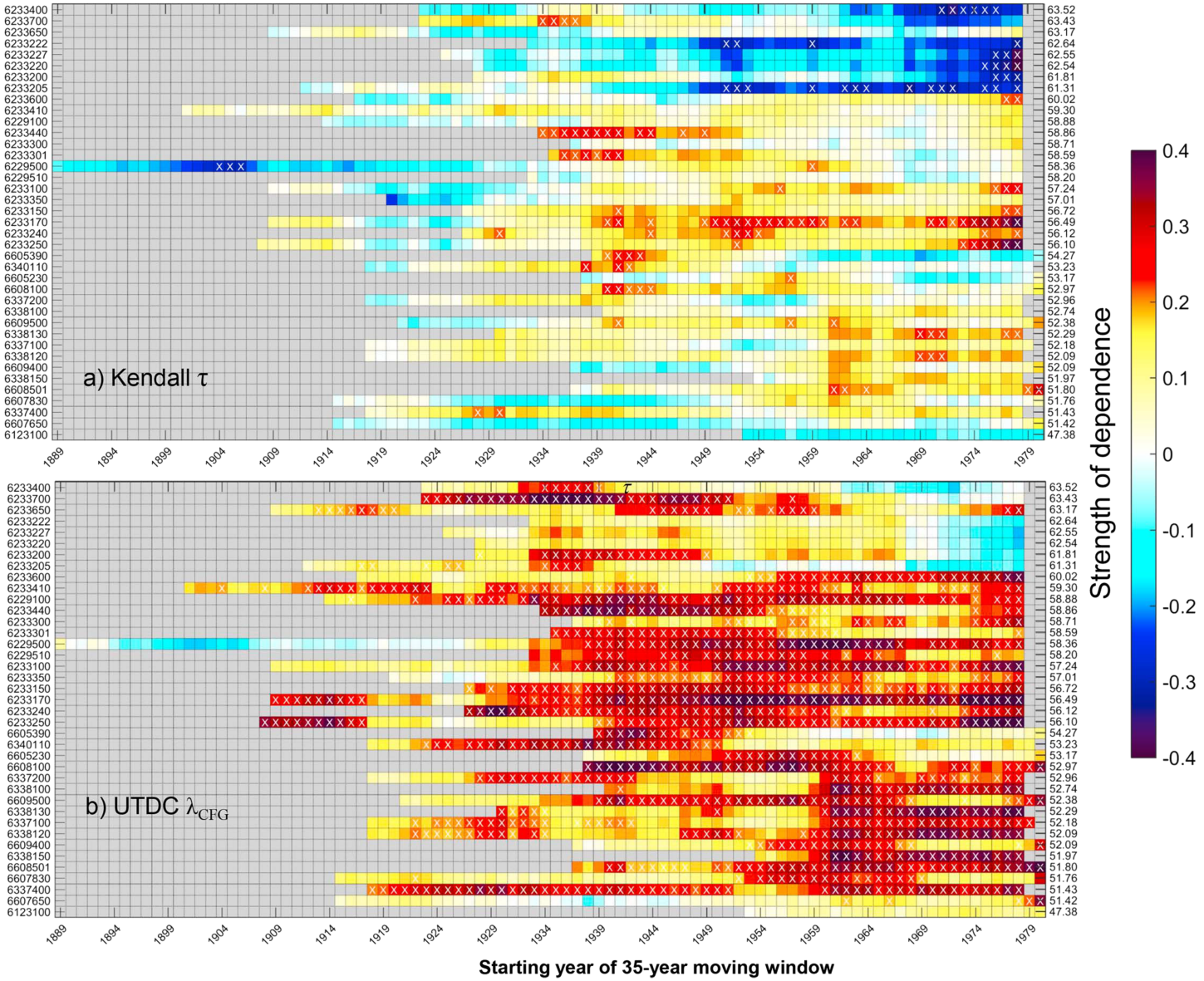

Figure 2. Temporal evolution of strength of dependence across latitude. The dependence at individual stream gauge locations is shown using heat maps. The top panel (a) shows total correlation as estimated using the rank-based Kendall's τ, whereas the bottom panel (b) shows the empirical upper tail dependence estimated using the Capéraá-Fougéres-Genest estimator, λ_{CFG}. The cells with significant dependence (i.e., p value < 0.05) are marked with "x" symbols in white. The x axis labels at the left shows the Global Runoff Data Centre station number, arranged from south (Gauge ID: 6123100, Loire France) to North (Gauge ID: 6233400, Fyrsjoen, Sweden) across the latitude (the x axis labels at the right).

To understand the space-time variability of dependence, we present heat maps (Figure 2) of dependence between HCWL and peak discharge as observed during the ±7-day window at each SG location, ordered along latitude. We find coherent dependence patterns, with a typically strong positive dependence at the upper tail across all latitudes (Figure 2b). We can delineate three distinct regions: (Region I) Below 52°N latitude, the positive dependence values tend to be stronger after 1960s. (Region II) From 52° to 60°N latitude, the strength of dependence tends to be constantly high. (Region III) Above 60°N latitude, the upper tail dependence is somewhat lower and decreases during the recent decades. Similar patterns are also observed in the total correlation (Kendall's τ) metrics, however, with lower correlation values (Figure 2a). To summarize, we find weaker dependence for the high-latitude SGs along the Northern Baltic coast and identify three regions with different, and partially contrasting, temporal evolution of dependence.

This increase in correlation could be a result of RSL rise in the North Sea, since higher coastal water levels can affect river flooding by altering tidal ranges in rivers, as HCWL can further propagate inland (Alvarado-Aguilar et al., 2012; Marsh & Schmidt, 1993). Region II is located on the west facing coasts, that is, western coasts of the United Kingdom, Germany, Netherlands, and Sweden. The strong dependence of the western coasts could be a consequence of the orographically enhanced precipitation associated with southwesterly airflow and cyclones traveling northeastward (Svensson & Jones, 2001; Svensson & Jones, 2004). On the other hand, gauges at Region I are mostly streams in the interior of the continent (e.g., Loire in France) and often located in east facing coasts that show weak to moderate dependency (Paprotny et al., 2018). The weak to negative dependency in the River Thames at Kingstone (Gauge ID: 6607650) may be caused by strong anthropogenic influences, such as large abstractions to meet London's water supply demand (Hannaford & Marsh, 2006). However, an increase in correlations in these gauges after 1960s could be attributed to the decadal rise in RSLs across the North Sea as observed in the increasing trend in the location parameters at Newlyn and Cuxhaven (Figure S2, left panel). Further, increasing runoff since the early 1960s in Wales and Western England was reported in the literature (Hannaford & Marsh, 2006), which in turn affects trend in compound flooding. The weaker correlation values of SGs at Region III corroborates with Paprotny et al. (2018) that reported rare occurrences of compound flooding along most of the Nordic countries.

3.2. Regional Variability in Compound Flood Magnitude

To understand regional variability of compound floods, first we compare spatial trends in seasonal (November–March) peak discharge (unconditional) versus the CHR index (considering HCWLs at the middle year of each sliding window as conditioning flood driver) for 50- and 100-year return levels. Statistical significance of trends is computed using the nonparametric Mann-Kendall test statistics at 5% significance level. The trends in seasonal flood events and compound flood index show disparate spatial patterns (Figure S8). For the 50-year seasonal maxima events, the number of stations with significant downward trends (18 out of 37) is higher than the number of stations with significant upward trends (14 out of 37). Likewise, for 100-year seasonal maxima events, we note a smaller number of gauges with significant upward trends (13 out of 37) as compared to downward trends (20 out of 37). The difference in number of gauges showing down/upward changes in seasonal maxima is rather small. Applying a false discovery rate-based field significance test (Benjamini & Yekutieli, 2001) at both return levels, we found the upward trend in seasonal maxima is field significant (at 5% significance level) only at Region III, whereas the downward trend is field significant over all regions (Table S2). In contrast, considering CHR series, the number of stations showing significant upward trends in flood magnitude is comparable to the number of stations with significant downward trends (14 out of 37 and 15 out of 37 for 50- and 100-year return events, respectively). Likewise, upward trends in CHR are field significant at Regions I and II, whereas downward trends are field significant over Regions II and III (Table S2).

3.3. Contrasting Response of Compound Flood Frequency in Middle Versus High Latitudes

Besides analyzing trends in magnitude, we compare changes in the frequency (i.e., counts) of compound floods, using a threshold, CHR > 1 (section 2). The compound flood frequency across the latitude (Figure 3, left) shows no consistent change for 50-year events. For 100-year events, an overall decrease in the number of events is interrupted by a modest increase in gauges located between 53°N and 57°N latitude. Overall, we note that a large number of compound events (a few of them are outliers and are not captured by ±2 standard deviation bounds) occur in Region II, which could be due to the high dependence values between its drivers.

The temporal evolution of CHR frequency indicates a moderate to sharp increase in the count of CHR for gauges below 60°N latitude (Figure 3, middle panel) in the decade centered on 1960s and decrease thereafter. This may be a consequence of the increasing dependence for the gauges below ~52°N latitude (Figure 2) during this period and of the interdecadal variability of influencing drivers. As an additional perspective, we present heat maps of trends in peak discharge within ±7 days from the occurrence of the HCWL at individual SGs (Figure S9), which suggest signatures of decadal variability with an increase in peak discharge between post-1957 and pre-1970 and decrease thereafter for the SGs below 53°N latitude. The decadal trends in compound floods shown in Figure 3 are qualitatively similar to December–March average stream flow in northern and northern coastal European regions in Figure 9 of Hannaford et al. (2013), with the exception of

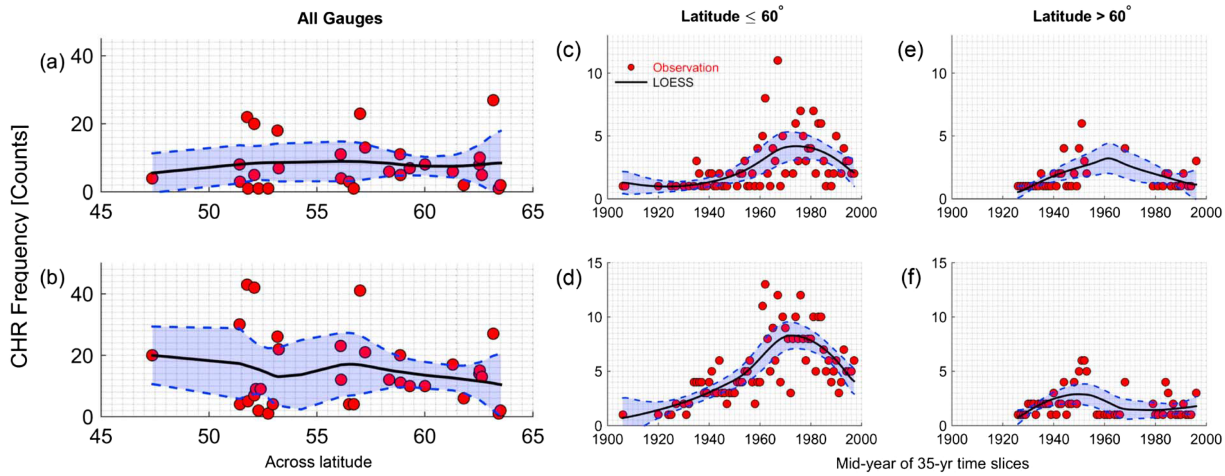

Figure 3. Changes in compound hazard ratio (CHR) frequency. The number of compound floods with CHR > 1, indicating potentially destructive events, are shown for the stream gauges across the space (a and b) and time (c–f) for the 50-year (top panel, a, c, and e) and 100-year (bottom panel, b, d, and f) events. The CHR frequency is smoothed using LOcally wEighted Scatter plot Smoothing (LOESS) regression (shown in black) with span length, 0.6. The uncertainty envelop (mean ± 2 × standard deviations) of the LOESS curve is obtained through $N = 1{,}000$ bootstrap samples.

the past decades 1940–1960, which shows lower variability in the mean stream flow trends. However, unlike Hannaford et al. (2013), we focus on peak discharge as a consequence of HCWL, and the larger variability in the CHR frequency could result from the lower number of gauges in the present study. The variability in compound flooding might be linked to the North Atlantic Oscillation, which influences rainfall, temperature, and streamflow in northern Europe, in particular during winter when the influence of North Atlantic Oscillation on regional hydroclimatology is found to be strongest (Chen et al., 2014; Hannaford et al., 2013; Steirou et al., 2019; Weisse et al., 2012). In contrast, Region III shows no detectable changes in CHR frequency.

4. Discussion and Implications for Regional Preparedness

The multitemporal evolution of dependence of compound flood drivers reveals that trends do not necessarily persist over very long periods but that there tend to be specific periods in which the dependence displays a stronger positive signal, implying stronger compound floods. The spatial pattern of the compound flood index suggests a coherent nature with (significant) increasing trends in compound flood magnitude for most of the gauges below 60°N latitude and (significant) decreasing trends for almost all gauges above 60°N latitude. The multidecadal evolution of compound flood suggests temporal clustering of events. We note an increase in the number of events at higher return levels with a sharp increase in the decade centered on 1960s, a compound flood-rich period between 1960s and 1980s, and a drop during 1990s for the gauges below 60°N latitude.

The presence of decadal and multidecadal variability in the magnitude and frequency of compound floods emphasizes the importance of including long records since the patterns obtained from short records could be confounded with climate change consequences. Identification of compound flood-rich and flood-poor periods and the corresponding group of SGs with increased probability of flooding, when the coast is hit by a severe storm, is highly relevant information for stakeholders such as government agencies and insurance companies. The coincidence of coastal and riverine flooding might stress disaster management much more compared to a situation, where comparable magnitudes of coastal and river flooding occur at different times. While the spatiotemporal coverage of observations remains constrained for this study, the results discussed herein provide a comprehensive view of compound flood trends in the study region. While our proof-of-principal results are shown for northwestern Europe utilizing its rich database, the framework could be transferred to quantify the space-time nature of compound flooding in any geographical location of the globe. No attempt has been made to relate the observed trends in compound floods to anthropogenic climate change or other human interventions; however, this could be a valuable future

research effort. Climate change is expected to increase the wind speed and intensify the rainfall intensity of severe storms (Patricola & Wehner, 2018). Global warming due to greenhouse gases could increase the severity and frequency of compound extremes (Zscheischler et al., 2018) by changes in wind speed and in rainfall intensity of severe storms. However, understanding the effects of such changes requires detailed analyses, as onshore and offshore winds, for example, might play opposite roles for compound floods. A formal hypothesis-driven research, based on a combination of climate-model simulations together with an analysis of observations, may augment our understanding of the role of human intervention on changes in compound flooding, which would provide valuable information for adaptation policies (Lin & Emanuel, 2016; Risser & Wehner, 2017).

Acknowledgments
We thank GRDC data center and GESLA (http://gesla.org/) for providing streamflow and sea level data, respectively. The first author would like to thank Marco Brettschneider, AXA Global P&C, Paris, France, for sharing the English version of the daily streamflow discharge data of River Loire from Banque Hydro website. Corresponding author, Dr. Poulomi Ganguli, is a recipient of *Humboldt Research Fellowship* for early career researchers from Alexander von Humboldt Foundation, Germany. Support from the foundation and the host institute, GFZ German Research Centre for Geosciences, Potsdam, Germany, is deeply acknowledged.

References

Alvarado-Aguilar, D., Jiménez, J. A., & Nicholls, R. J. (2012). Flood hazard and damage assessment in the Ebro Delta (NW Mediterranean) to relative sea level rise. *Natural Hazards*, *62*(3), 1301–1321. https://doi.org/10.1007/s11069-012-0149-x

Bartsch-Winkler, S., & Lynch, D. K. (1988). *Catalog of worldwide tidal bore occurrences and characteristics. (No. 1022)*. Denver, CO: US Government Printing Office.

Bender, J., Wahl, T., & Jensen, J. (2014). Multivariate design in the presence of non-stationarity. *Journal of Hydrology*, *514*, 123–130. https://doi.org/10.1016/j.jhydrol.2014.04.017

Benjamini, Y., & Yekutieli, D. (2001). The control of the false discovery rate in multiple testing under dependency. *The Annals of Statistics*, *29*(4), 1165–1188.

Berghuijs, W. R., Allen, S. T., Harrigan, S., & Kirchner, J. W. (2019). Growing spatial scales of synchronous river flooding in Europe. *Geophysical Research Letters*, *46*, 1423–1428. https://doi.org/10.1029/2018GL081883

Berne, A., Delrieu, G., Creutin, J.-D., & Obled, C. (2004). Temporal and spatial resolution of rainfall measurements required for urban hydrology. *Journal of Hydrology*, *299*(3-4), 166–179. https://doi.org/10.1016/S0022-1694(04)00363-4

Best, J. (2018). Anthropogenic stresses on the world's big rivers. *Nature Geoscience*, *12*, 7–21.

Bevacqua, E., Maraun, D., Hobæk Haff, I., Widmann, M., & Vrac, M. (2017). Multivariate statistical modelling of compound events via pair-copula constructions: Analysis of floods in Ravenna (Italy). *Hydrology and Earth System Sciences*, *21*(6), 2701–2723.

Bevacqua, E., Maraun, D., Vousdoukas, M. I., Voukouvalas, E., Vrac, M., Mentaschi, L., & Widmann, M. (2018). Higher potential compound flood risk in Northern Europe under anthropogenic climate change. https://doi.org/10.31223/osf.io/ta764

Brunetti, M., Maugeri, M., & Nanni, T. (2001). Changes in total precipitation, rainy days and extreme events in northeastern Italy. *International Journal of Climatology*, *21*(7), 861–871. https://doi.org/10.1002/joc.660

Brunner, M. I., Seibert, J., & Favre, A.-C. (2016). Bivariate return periods and their importance for flood peak and volume estimation. *Wiley Interdisciplinary Reviews Water*, *3*(6), 819–833. https://doi.org/10.1002/wat2.1173

Burn, D. H., & Whitfield, P. H. (2018). Changes in flood events inferred from centennial length streamflow data records. *Advances in Water Resources*, *121*, 333–349. https://doi.org/10.1016/j.advwatres.2018.08.017

Chen, X., Dangendorf, S., Narayan, N., O'Driscoll, K., Tsimplis, M. N., & Su, J. (2014). On sea level change in the North Sea influenced by the North Atlantic Oscillation: local and remote steric effects. *Estuarine, Coastal and Shelf Science*, *151*, 186–195.

Cheng, L., & AghaKouchak, A. (2014). Nonstationary precipitation intensity-duration-frequency curves for infrastructure design in a changing climate. *Scientific Reports*, *4*, srep07093.

Cheng, L., AghaKouchak, A., Gilleland, E., & Katz, R. W. (2014). Non-stationary extreme value analysis in a changing climate. *Climatic Change*, *127*(2), 353–369. https://doi.org/10.1007/s10584-014-1254-5

Chok, N. S. (2010). Pearson's versus Spearman's and Kendall's correlation coefficients for continuous data (PhD Thesis). University of Pittsburgh.

Coles, S. (2001). *An introduction to statistical modeling of extreme values*. London, Great Britain: Springer.

Couasnon, A., Sebastian, A., & Morales-Nápoles, O. (2018). A copula-based Bayesian network for modeling compound flood hazard from riverine and coastal interactions at the catchment scale: An application to the Houston Ship Channel, Texas. *Water*, *10*(9), 1190.

Czajkowski, J., Villarini, G., Montgomery, M., Michel-Kerjan, E., & Goska, R. (2017). Assessing current and future freshwater flood risk from North Atlantic tropical cyclones via insurance claims. *Scientific Reports*, *7*, 41609.

Di Baldassarre, G., & Montanari, A. (2009). Uncertainty in river discharge observations: A quantitative analysis. *Hydrology and Earth System Sciences*, *13*(6), 913–921. https://doi.org/10.5194/hess-13-913-2009

EEA (European Environment Agency). (2017). Global and European sea level. Retrieved from https://www.eea.europa.eu/data-and-maps/indicators/sea-level-rise-5/assessment

Feser, F., Barcikowska, M., Krueger, O., Schenk, F., Weisse, R., & Xia, L. (2015). Storminess over the North Atlantic and northwestern Europe—A review. *Quarterly Journal of the Royal Meteorological Society*, *141*(687), 350–382. https://doi.org/10.1002/qj.2364

Field, C. B., Barros, V., Stocker, T. F., & Dahe, Q. (2012). *Managing the risks of extreme events and disasters to advance climate change adaptation: Special report of the intergovernmental panel on climate change*. Cambridge: Cambridge University Press. https://doi.org/10.1017/CBO9781139177245

Ganguli, P., & Ganguly, A. (2016). Space-time trends in U.S. meteorological droughts. *Journal of Hydrology: Regional Studies*, *8*, 235–259.

Ghosh, S., Das, D., Kao, S.-C., & Ganguly, A. R. (2012). Lack of uniform trends but increasing spatial variability in observed Indian rainfall extremes. *Nature Climate Change*, *2*(2), 86–91. https://doi.org/10.1038/nclimate1327

Grabs, W. (1997). Report on the Third Meeting of the GRDC Steering Committee: Koblenz, Germany, 25-27 June 1997.

Gudmundsson, L., Leonard, M., Do, H. X., Westra, S., & Seneviratne, S. I. (2018). Observed trends in global indicators of mean and extreme streamflow. *Geophysical Research Letters*, *46*, 756–766. https://doi.org/10.1029/2018GL079725

Haigh, I. D., Wadey, M. P., Wahl, T., Ozsoy, O., Nicholls, R. J., Brown, J. M., et al. (2016). Spatial and temporal analysis of extreme sea level and storm surge events around the coastline of the UK. *Scientific Data*, *3*(1), 160107. https://doi.org/10.1038/sdata.2016.107

Hannaford, J., Buys, G., Stahl, K., & Tallaksen, L. M. (2013). The influence of decadal-scale variability on trends in long European streamflow records. *Hydrology and Earth System Sciences*, *17*(7), 2717–2733. https://doi.org/10.5194/hess-17-2717-2013

Hannaford, J., & Marsh, T. (2006). An assessment of trends in UK runoff and low flows using a network of undisturbed catchments. *International Journal of Climatology*, *26*(9), 1237–1253. https://doi.org/10.1002/joc.1303

Hidayat, H., Vermeulen, B., Sassi, M. G., Torfs, P. J. J. F., & Hoitink, A. J. F. (2011). Discharge estimation in a backwater affected meandering river. *Hydrology and Earth System Sciences*, *15*(8), 2717–2728. https://doi.org/10.5194/hess-15-2717-2011

Hoitink, A. J. F., & Jay, D. A. (2016). Tidal river dynamics: Implications for deltas. *Reviews of Geophysics*, *54*, 240–272. https://doi.org/10.1002/2015RG000507

Holtan, H. N., & Overton, D. E. (1963). Analyses and application of simple hydrographs. *Journal of Hydrology*, *1*(3), 250–264. https://doi.org/10.1016/0022-1694(63)90005-2

Kew, S. F., Selten, F. M., Lenderink, G., & Hazeleger, W. (2013). The simultaneous occurrence of surge and discharge extremes for the Rhine delta. *Natural Hazards and Earth System Sciences*, *13*(8), 2017–2029. https://doi.org/10.5194/nhess-13-2017-2013

Kharin, V. V., Zwiers, F. W., Zhang, X., & Hegerl, G. C. (2007). Changes in temperature and precipitation extremes in the IPCC ensemble of global coupled model simulations. *Journal of Climate*, *20*(8), 1419–1444. https://doi.org/10.1175/JCLI4066.1

Klerk, W. J., Winsemius, H. C., van Verseveld, W. J., Bakker, A. M. R., & Diermanse, F. L. M. (2015). The co-incidence of storm surges and extreme discharges within the Rhine–Meuse Delta. *Environmental Research Letters*, *10*(3), 035005. https://doi.org/10.1088/1748-9326/10/3/035005

Kwadijk, J., Arnell, N. W., Mudersbach, C., de Weerd, M., Kroon, A., & Quante, M. (2016). Recent change—River flow. In *North Sea Region Climate Change Assessment* (pp. 137–146). Cham: Springer. https://doi.org/10.1007/978-3-319-39745-0_4

Leonard, M., Westra, S., Phatak, A., Lambert, M., van den Hurk, B., McInnes, K., et al. (2014). A compound event framework for understanding extreme impacts. *Wiley Interdisciplinary Reviews: Climate Change*, *5*(1), 113–128.

Leopold, L. B. (1991). Lag times for small drainage basins. *Catena*, *18*(2), 157–171. https://doi.org/10.1016/0341-8162(91)90014-O

Lian, J., Xu, K., & Ma, C. (2013). Joint impact of rainfall and tidal level on flood risk in a coastal city with a complex river network: a case study of Fuzhou City, China. *Hydrology and Earth System Sciences*, *17*(2), 679–689. https://doi.org/10.5194/hess-17-679-2013

Lin, N., & Emanuel, K. (2016). Grey swan tropical cyclones. *Nature Climate Change*, *6*(1), 106–111. https://doi.org/10.1038/nclimate2777

Mangini, W., Viglione, A., Hall, J., Hundecha, Y., Ceola, S., Montanari, A., et al. (2018). Detection of trends in magnitude and frequency of flood peaks across Europe. *Hydrological Sciences Journal*, *63*(4), 493–512. https://doi.org/10.1080/02626667.2018.1444766

Marsh, P., & Schmidt, T. (1993). Influence of a Beaufort Sea storm surge on channel levels in the Mackenzie Delta. *Arctic*, 35–41.

Martins, E. S., & Stedinger, J. R. (2000). Generalized maximum-likelihood generalized extreme-value quantile estimators for hydrologic data. *Water Resources Research*, *36*(3), 737–744. https://doi.org/10.1029/1999WR900330

Meade, R. H., & Emery, K. (1971). Sea level as affected by river runoff, eastern United States. *Science*, *173*(3995), 425–428. https://doi.org/10.1126/science.173.3995.425

Mediero, L., Kjeldsen, T. R., Macdonald, N., Kohnova, S., Merz, B., Vorogushyn, S., et al. (2015). Identification of coherent flood regions across Europe by using the longest streamflow records. *Journal of Hydrology*, *528*, 341–360. https://doi.org/10.1016/j.jhydrol.2015.06.016

Melet, A., Meyssignac, B., Almar, R., & Cozannet, G. L. (2018). Under-estimated wave contribution to coastal sea-level rise. *Nature Climate Change*, *8*(3), 234–239. https://doi.org/10.1038/s41558-018-0088-y

Merz, B., Dung, N. V., Apel, H., Gerlitz, L., Schröter, K., Steirou, E., & Vorogushyn, S. (2018). Spatial coherence of flood-rich and flood-poor periods across Germany. *Journal of Hydrology*, *559*, 813–826. https://doi.org/10.1016/j.jhydrol.2018.02.082

Moftakhari, H., Schubert, J. E., AghaKouchak, A., Matthew, R. A., & Sanders, B. F. (2019). Linking statistical and hydrodynamic modeling for compound flood hazard assessment in tidal channels and estuaries. *Advances in Water Resources*, *128*, 28–38. https://doi.org/10.1016/j.advwatres.2019.04.009

Moftakhari, H. R., Salvadori, G., AghaKouchak, A., Sanders, B. F., & Matthew, R. A. (2017). Compounding effects of sea level rise and fluvial flooding. *Proceedings of the National Academy of Sciences*, *114*(37), 9785–9790. https://doi.org/10.1073/pnas.1620325114

Nelsen, R. B. (2013). *An introduction to copulas*. New York: Springer.

Neumann, B., Vafeidis, A. T., Zimmermann, J., & Nicholls, R. J. (2015). Future coastal population growth and exposure to sea-level rise and coastal flooding—a global assessment. *PLoS ONE*, *10*(3), e0118571. https://doi.org/10.1371/journal.pone.0118571

Ntegeka, V., & Willems, P. (2008). Trends and multidecadal oscillations in rainfall extremes, based on a more than 100-year time series of 10 min rainfall intensities at Uccle, Belgium. *Water Resources Research*, *44*, W07402. https://doi.org/10.1029/2007WR006471

Paprotny, D., Vousdoukas, M. I., Morales-Nápoles, O., Jonkman, S. N., & Feyen, L. (2018). Compound flood potential in Europe. *Hydrology and Earth System Sciences Discussions*, 1–34. https://doi.org/10.5194/hess-2018-132

Patricola, C. M., & Wehner, M. F. (2018). Anthropogenic influences on major tropical cyclone events. *Nature*, *563*(7731), 339–346. https://doi.org/10.1038/s41586-018-0673-2

Pescaroli, G., & Alexander, D. (2018). Understanding compound, interconnected, interacting, and cascading risks: A holistic framework. *Risk Analysis*, *38*(11), 2245–2257. https://doi.org/10.1111/risa.13128

Petroliagkis, T. I., Voukouvalas, E., Disperati, J., & Bidlot, J. (2016). Joint probabilities of storm surge, significant wave height and river discharge components of coastal flooding events. *European Commission-JRC Technical Reports*, EUR 27824 EN, 1-84.

Piecuch, C. G., Bittermann, K., Kemp, A. C., Ponte, R. M., Little, C. M., Engelhart, S. E., & Lentz, S. J. (2018). River-discharge effects on United States Atlantic and Gulf coast sea-level changes. *Proceedings of the National Academy of Sciences*, *115*(30), 7729–7734. https://doi.org/10.1073/pnas.1805428115

Reeve, D. E., Rozynski, G., & Li, Y. (2008). Extreme water levels of the Vistula River and Gdansk Harbour. *Journal of Hydraulic Research*, *46*(sup2), 235–245. https://doi.org/10.1080/00221686.2008.9521957

Richter, K., Nilsen, J., & Drange, H. (2012). Contributions to sea level variability along the Norwegian coast for 1960–2010. *Journal of Geophysical Research*, *117*, C05038. https://doi.org/10.1029/2011JC007826

Risser, M. D., & Wehner, M. F. (2017). Attributable human-induced changes in the likelihood and magnitude of the observed extreme precipitation during hurricane Harvey. *Geophysical Research Letters*, *44*, 12,457–12,464. https://doi.org/10.1002/2017GL075888

Rowe, S. T., & Villarini, G. (2013). Flooding associated with predecessor rain events over the Midwest United States. *Environmental Research Letters*, *8*(2), 024007.

Sadegh, M., Moftakhari, H., Gupta, H. V., Ragno, E., Mazdiyasni, O., Sanders, B., et al. (2018). Multihazard scenarios for analysis of compound extreme events. *Geophysical Research Letters*, *45*, 5470–5480. https://doi.org/10.1029/2018GL077317

Smith, J. A., Villarini, G., & Baeck, M. L. (2011). Mixture distributions and the hydroclimatology of extreme rainfall and flooding in the eastern United States. *Journal of Hydrometeorology*, *12*(2), 294–309.

Steirou, E., Gerlitz, L., Apel, H., Sun, X., & Merz, B. (2019). Climate influences on flood probabilities across Europe. *Hydrology and Earth System Sciences*, *23*(3), 1305–1322. https://doi.org/10.5194/hess-23-1305-2019

Stocker, T. F. (2014). *Climate change 2013: The physical science basis: Working Group I contribution to the Fifth Assessment Report of the Intergovernmental Panel on Climate Change*, (p. 1535). Cambridge, New York, USA: Cambridge University Press.

Svensson, C., & Jones, D. A. (2001). Dependence between sea surge, river flow and precipitation in south and west Britain. *Hydrology and Earth System Sciences*, *8*(5), 973–992.

Svensson, C., & Jones, D. A. (2004). Dependence between sea surge, river flow and precipitation in south and west Britain. *Hydrology and Earth System Sciences Discussions*, *8*(5), 973–992. https://doi.org/10.5194/hess-8-973-2004

Sweet, W. V., Dusek, G. P., Obeysekera, J. T. B., & Marra, J. J. (2018). Patterns and projections of high tide flooding along the US coastline using a common impact threshold. National Oceanic and Atmospheric Administration, Technical Report no. NOS CO-OPS 086, 1-56, 2018.

Tawn, J. A. (1992). Estimating probabilities of extreme sea-levels. *Journal of the Royal Statistical Society: Series C: Applied Statistics*, *41*(1), 77–93.

Tu, X., Du, Y., Singh, V. P., & Chen, X. (2018). Joint distribution of design precipitation and tide and impact of sampling in a coastal area. *International Journal of Climatology*, *38*, e290–e302. https://doi.org/10.1002/joc.5368

Villarini, G., & Smith, J. A. (2010). Flood peak distributions for the eastern United States. *Water Resources Research*, *46*, W06504. https://doi.org/10.1029/2009WR008395

Wahl, T., Haigh, I. D., Woodworth, P. L., Albrecht, F., Dillingh, D., Jensen, J., et al. (2013). Observed mean sea level changes around the North Sea coastline from 1800 to present. *Earth-Science Reviews*, *124*, 51–67.

Wahl, T., Jain, S., Bender, J., Meyers, S. D., & Luther, M. E. (2015). Increasing risk of compound flooding from storm surge and rainfall for major US cities. *Nature Climate Change*, *5*(12), 1093–1097. https://doi.org/10.1038/nclimate2736

Ward, P. J., Couasnon, A., Eilander, D., Haigh, I., Hendry, A., Muis, S., et al. (2018). Dependence between high sea-level and high river discharge increases flood hazard in global deltas and estuaries. *Environmental Research Letters*, *13*(8). https://doi.org/10.1088/1748-9326/aad400

Weisse, R., von Storch, H., Niemeyer, H.D., & Knaack, H. (2012). Changing North Sea storm surge climate: an increasing hazard? *Ocean & Coastal Management*, *68*, 58–68.

Woodworth, P. L., Hunter, J. R., Marcos Moreno, M., Caldwell, P. C., Menendez, M., & Haigh, I. D. (2016). GESLA (Global Extreme Sea Level Analysis) high frequency sea level dataset—Version 2.UK: British Oceanographic Data Centre - Natural Environment Research Council. DOI: 10/bp74, Retrieved from http://www.gesla.org/

World Meteorological Organization [WMO] (2017). WMO guidelines on the calculation of climate normals. World Meteorological Organization Geneva. WMO Technical Report, WMO-No. 1203, 1-29.

Wu, W., McInnes, K., O'Grady, J., Hoeke, R., Leonard, M., & Westra, S. (2018). Mapping dependence between extreme rainfall and storm surge. *Journal of Geophysical Research: Oceans*, *123*, 2461–2474. https://doi.org/10.1002/2017JC013472

Zheng, F., Leonard, M., & Westra, S. (2017). Application of the design variable method to estimate coastal flood risk. *Journal of Flood Risk Management*, *10*(4), 522–534.

Zheng, F., Westra, S., Leonard, M., & Sisson, S. A. (2014). Modeling dependence between extreme rainfall and storm surge to estimate coastal flooding risk. *Water Resources Research*, *50*, 2050–2071. https://doi.org/10.1002/2013WR014616

Zheng, F., Westra, S., & Sisson, S. A. (2013). Quantifying the dependence between extreme rainfall and storm surge in the coastal zone. *Journal of Hydrology*, *505*, 172–187. https://doi.org/10.1016/j.jhydrol.2013.09.054

Zscheischler, J., Westra, S., Hurk, B. J., Seneviratne, S. I., Ward, P. J., Pitman, A., et al. (2018). Future climate risk from compound events. *Nature Climate Change*, *8*, 469–477.